Semiconductor Physics, Quantum Electronics & Optoelectronics, 2024. V. 27, No 3. P. 328-336.

Optoelectronics and optoelectronic devices

Tight focusing of terahertz vortex beams formed by laser dielectric resonator

A.V. Degtyarev, M.M. Dubinin*, V.O. Maslov, K.I. Muntean, O.O. Svystunov

V.N. Karazin Kharkiv National University, 4 Svobody Square, 61022 Kharkiv, Ukraine
**Corresponding author e-mail: mykola.dubinin@karazin.ua*

Abstract. Wave characteristics of vortex laser beams during their tight focusing have been theoretically studied. The Rayleigh–Sommerfeld theory was used to describe propagation in free space of laser beams excited by the modes of a waveguide dielectric resonator. It is shown that at the topological charge of the spiral phase plate $n = 0$, the studied EH_{11} mode has a maximum of radiation intensity on the axis. Introduction of a topological charge leads to the appearance of a minimum of radiation intensity on the axis as well as to the increase in the size of the focal spot. However, for the TE_{01} mode with the topological charges $n = 0$ and $n = 2$, the intensity distribution retains a ring shape, while at $n = 1$ the beam profile turns into the Gaussian-like one. The wave front in the focal region of the lens for the components of the EH_{11} and TE_{01} modes transforms from spherical to spiral one with increasing the topological charge.

Keywords: vortex beams, terahertz laser, dielectric resonator, modes, tight focusing.

https://doi.org/10.15407/spqeo27.03.328
PACS 42.55.-f, 42.60.Da, 42.60.-v, 42.62.-b

Manuscript received 28.05.24; revised version received 20.07.24; accepted for publication 11.09.24; published online 20.09.24.

1. Introduction

In recent decades, the problems of formation, propagation and focusing of terahertz (THz) wave beams have been actively considered [1–3]. At this, vortex laser beams play an important role due to their uniqueness. Their feature is the spiral structure of the wavefront, which ensures presence of an orbital wave momentum with a large number of states and additional degrees of freedom [4–6]. Vortex laser beams have great potential for application in high-speed multiplex THz communication systems, tomography, materials research, electron bunch acceleration and astrophysics [7–11].

The key methods for generating terahertz vortex beams use two principles: wavefront modulation using special external devices and direct excitation of vortex beams at the resonator output. Extracavity wavefront modulation methods are based on a wide range of optical elements, including spiral phase plates, achromatic polarization elements and computer holograms [12–19]. On the other hand, direct excitation of vortex beams in a laser cavity can be accomplished through optical rectification and multi-frequency generation [20–22].

One of the most well-known optical elements for creating vortex beams is a spiral phase plate with an azimuthally varying thickness [23]. This element works by directly imposing a helical phase shift on the incident laser beam, effectively converting virtually all of the incident radiation energy into a vortex beam.

Focused vortex beams with a spiral distribution of the wavefront phases reveal features that are absent in conventional Gaussian beams. These properties of vortex beams can be applied in a wide range of industries, including quantum information processing [24], astronomical detection [25] and optical processing [26]. Moreover, when a focused vortex beam with a predetermined focal plane acts on a particle, the orbital angular momentum carried by the beam can be transferred to the particle. This process provides a high degree of flexibility to manipulate the rotation and movement of this particle [27].

Studies of the properties of tightly focused vortex beams have attracted attention of many scientists in recent years, because they make it possible not only to obtain a focal spot that does not diverge at a certain distance, but also to change the coherence of the incident light [28]. It has been shown that the intensity distribution near the focus as well as the corresponding angular orbital momentum depend not only on the numerical aperture and initial polarization angle, but also on the topological charge of the vortex beam [29]. Moreover, tight focusing of linearly, radially and

azimuthally polarized light demonstrates a number of non-trivial effects, such as the Hall effect and others [30–34]. However, all these studies were carried out in the optical range.

There are only a few known works that study focusing of vortex beams in the terahertz range. In [35], a series of spintronic terahertz emitters with a spiral Fresnel zone plate was developed to directly generate focused terahertz vortex beams with different topological charges. The authors [36] proposed a metasurface that can be used to focus incident waves with arbitrary polarization states into a vortex beam carrying the same topological charge.

In these studies, broadband radiation from subpicosecond pulse generators based on femtosecond lasers is used. This approach leads to difficulties in the production of laser systems, and the effects of the interaction of pulsed radiation with matter are significantly different from the effects characteristic of continuous radiation. Molecular lasers with optical pumping are currently the only compact sources of continuous terahertz radiation that can be discretely tunable over the entire terahertz range and have a narrow spectral line. Increasing interest in such sources is associated with the possibility of using tunable mid-IR quantum cascade lasers to pump them [37]. Molecular lasers often use waveguide resonators, which make it possible to obtain a power of up to 1 W in a continuous regime at relatively small cavity sizes [38]. Among the resonator modes, the EH_{11} mode with linear polarization and the TE_{01} mode with azimuthal polarization have the lowest energy losses [39].

The purpose of this work is to obtain analytical expressions for describing the components of the radiation fields formed by the modes of a waveguide dielectric resonator of a terahertz laser in the focal region of the lens as well as to study the physical features of the obtained vortex beams when they are tightly focused.

2. Theoretical relations

Propagation of laser radiation in a free space along the 0z axis is described by the well-known Rayleigh–Sommerfeld integrals. We use the following expressions for the field components in a cylindrical coordinate system in different diffraction zones [40]:

where $k = 2\pi/\lambda$ is the wave number, λ is the wavelength, (ρ_0, φ) are the polar coordinates in the region where the input field is specified, and $E_x^0(\rho_0, \varphi)$ and $E_y^0(\rho_0, \varphi)$ are the complex amplitudes of the x and y components of the input electric field, respectively, $r_1 = \sqrt{\rho_1^2 + z_1^2}$.

The modes of the studied dielectric resonator coincide with the modes of a hollow circular dielectric waveguide. Therefore, in the initial plane we define radiation in the form of symmetric linearly and azimuthally polarized EH_{11} and TE_{01} modes, respectively. The expressions for the Cartesian components of electromagnetic fields of these modes in the source plane $z = 0$ have the following form [39]:

EH_{11} mode

$$\begin{cases} E_x^0(\rho_0, \varphi) = 0, \\ E_y^0(\rho_0, \varphi) = A_{11} J_0\left(U_{11} \dfrac{\rho_0}{a}\right), \end{cases} \tag{2}$$

TE_{01} mode

$$\begin{cases} E_x^0(\rho_0, \varphi) = -B_{01} J_1\left(U_{01} \dfrac{\rho_0}{a}\right) \sin\varphi, \\ E_y^0(\rho_0, \varphi) = B_{01} J_1\left(U_{01} \dfrac{\rho_0}{a}\right) \cos\varphi, \end{cases} \tag{3}$$

where a is the radius of the waveguide, J_0 and J_1 are the Bessel functions of the first kind, U_{11} and U_{01} are the first roots of the equations $J_0(x) = 0$ and $J_1(x) = 0$, respectively, $A_{11} = \dfrac{1}{a\sqrt{\pi}\, J_1(U_{11})}$ and $B_{01} = \dfrac{1}{a\sqrt{\pi}\, J_2(U_{01})}$ are the normalizing factors for the EH_{11} and TE_{01} modes, respectively.

Consider the interaction of these modes with a spiral phase plate (SPP) with an arbitrary topological charge (n) [41]. Let us place the SPP with an aperture of the same radius a at the output of a waveguide (Fig. 1). The complex transmittance function of this SPP in polar coordinates has the following form [5]:

$$T_n(\rho_0, \varphi) = \mathrm{circ}\left(\frac{\rho_0}{a}\right) \exp(in\varphi) = \begin{cases} \exp(in\varphi), & \rho_0 \le a, \\ 0, & \rho_0 > a, \end{cases} \tag{4}$$

where $\mathrm{circ}\left(\dfrac{\rho_0}{a}\right)$ is the circular function.

$$E_x(\rho_1, \beta, z_1) = -\frac{iz_1}{\lambda r_1^2} \exp(ikr_1) \int_0^{\infty} \int_0^{2\pi} E_x^0(\rho_0, \varphi) \exp\left(ik \frac{\rho_0^2}{2r_1}\right) \exp\left(-ik \frac{\rho_1 \rho_0 \cos(\varphi - \beta)}{r_1}\right) \rho_0 \, d\rho_0 \, d\varphi, \tag{1.1}$$

$$E_y(\rho_1, \beta, z_1) = -\frac{iz_1}{\lambda r_1^2} \exp(ikr_1) \int_0^{\infty} \int_0^{2\pi} E_y^0(\rho_0, \varphi) \exp\left(ik \frac{\rho_0^2}{2r_1}\right) \exp\left(-ik \frac{\rho_1 \rho_0 \cos(\varphi - \beta)}{r_1}\right) \rho_0 \, d\rho_0 \, d\varphi, \tag{1.2}$$

$$E_z(\rho_1, \beta, z_1) = \frac{i}{\lambda r_1^2} \exp(ikr_1) \int_0^{\infty} \int_0^{2\pi} \left[E_x^0(\rho_0, \varphi)(\rho_1 \cos\beta - \rho_0 \cos\varphi) + E_y^0(\rho_0, \varphi)(\rho_1 \sin\beta - \rho_0 \sin\varphi)\right] \times$$
$$\times \exp\left(ik \frac{\rho_0^2}{2r_1}\right) \exp\left(-ik \frac{\rho_1 \rho_0 \cos(\varphi - \beta)}{r_1}\right) \rho_0 \, d\rho_0 \, d\varphi. \tag{1.3}$$

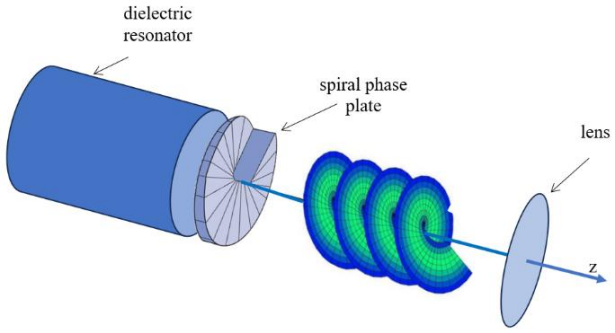

Fig. 1. Scheme of the calculation model of laser beam focusing.

To simplify the calculations, integration over the angle φ in (3) may be performed using the known relationships for the integer $m > 0$ from [42]:

$$\int_0^{2\pi} \cos(m\varphi+\varphi_0)\exp[-ix\cos(\varphi-\theta)d\varphi] = 2\pi(-i)^m J_m(x)\cos(m\varphi+\varphi_0),$$

$$\int_0^{2\pi} \sin(m\varphi+\varphi_0)\exp[-ix\cos(\varphi-\theta)d\varphi] = 2\pi(-i)^m J_m(x)\sin(m\varphi+\varphi_0).$$

We can get the following relation from here:

$$\int_0^{2\pi} e^{-ix\cos(\varphi-\beta)} e^{in\varphi} d\varphi = 2\pi e^{in\beta}(-i)^n J_n(x). \quad (5)$$

Using the Euler formulas and taking into account Eq. (5), we obtain the following expressions:

$$\int_0^{2\pi} e^{-ix\cos(\varphi-\beta)} e^{in\varphi}\sin\varphi d\varphi = -\pi e^{in\beta}(-i)^n\left[e^{i\beta}J_{n+1}(x)+e^{-i\beta}J_{n-1}(x)\right], \quad (6.1)$$

$$\int_0^{2\pi} e^{-ix\cos(\varphi-\beta)} e^{in\varphi}\cos\varphi d\varphi = \pi e^{in\beta}(-i)^{n+1}\left[e^{i\beta}J_{n+1}(x)-e^{-i\beta}J_{n-1}(x)\right]. \quad (6.2)$$

Substituting the expression for the complex transmittance function of the SPP (4) into (1) and using the formulas (5) and (6.1), we obtain the expressions for the field components that describe nonparaxial diffraction of the EH_{11} mode by SPP with a topological charge n in a free space at a distance z_1 from the end of the waveguide:

$$E_x(\rho_1,\beta,z_1) = 0, \quad (7.1)$$

$$E_y(\rho_1,\beta,z_1) = \frac{(-i)^{n+1}kz_1}{r_1^2}\exp[i(n\beta+kr_1)]A_{11}G1_{0n}(\rho_1,z_1), \quad (7.2)$$

$$E_z(\rho_1,\beta,z_1) = \frac{(-i)^{n+1}kz_1}{2r_1^2}\exp[i(n\beta+kr_1)]\times \times A_{11}\left\{\begin{matrix}2\rho_1\sin\beta G1_{0n}(\rho_1,z_1)+\exp(i\beta)H1_{0n+1}(\rho_1,z_1)+\\ +\exp(-i\beta)H1_{0n-1}(\rho_1,z_1)\end{matrix}\right\}, \quad (7.3)$$

where the following notations are introduced:

$$G1_{0n}(\rho_1,z_1) = \int_0^a J_0\left(U_{11}\frac{\rho_0}{a}\right)\exp\left(ik\frac{\rho_0^2}{2r_1}\right)J_n\left(\frac{k\rho_1\rho_0}{r_1}\right)\rho_0\, d\rho_0,$$

$$H1_{0n}(\rho_1,z_1) = \int_0^a J_0\left(U_{11}\frac{\rho_0}{a}\right)\exp\left(ik\frac{\rho_0^2}{2r_1}\right)J_n\left(\frac{k\rho_1\rho_0}{r_1}\right)\rho_0^2\, d\rho_0.$$

Also, using the formulas (6.1) and (6.2), we obtain the following expressions for the field components that describe nonparaxial diffraction of the TE_{01} mode on the SPP:

$$E_x(\rho_1,\beta,z_1) = \frac{(-i)^{n+1}kz_1}{r_1^2}\exp[i(n\beta+kr_1)]\times \times B_{01}[\exp(i\beta)G2_{1n+1}(\rho_1,z_1)+\exp(-i\beta)G2_{1n-1}(\rho_1,z_1)], \quad (8.1)$$

$$E_y(\rho_1,\beta,z_1) = \frac{(-i)^{n+2}kz_1}{2r_1^2}\exp[i(n\beta+kr_1)]\times \times B_{01}[\exp(i\beta)G2_{1n+1}(\rho_1,z_1)-\exp(-i\beta)G2_{1n-1}(\rho_1,z_1)], \quad (8.2)$$

$$E_z(\rho_1,\beta,z_1) = \frac{(-i)^{n+1}k\rho_1}{2r_1^2}\exp[i(n\beta+kr_1)]\times \times B_{01}[G2_{1n+1}(\rho_1,z_1)+G2_{1n-1}(\rho_1,z_1)], \quad (8.3)$$

where the following notation is introduced:

$$G2_{1n}(\rho_1,z_1) = \int_0^a J_1\left(U_{01}\frac{\rho_0}{a}\right)\exp\left(ik\frac{\rho_0^2}{2r_1}\right)J_n\left(\frac{k\rho_1\rho_0}{r_1}\right)\rho_0\, d\rho_0.$$

We describe the field at the input and output of a lens using the phase correction function $U(\rho_1)=\exp\left(\frac{-i\pi\rho_1^2}{\lambda F}\right)$, where F is the focal length of the lens. By applying again the Rayleigh–Sommerfeld integral transformations (1) to the components of the electric field strength vector (7) and (8), found after phase correction, we obtain the analytical expressions for the transverse and longitudinal field components of the studied modes in the focal region of the lens.

The field components for the linearly polarized EH_{11} mode at a distance z_2 from the lens have the following form:

$$E_x(\rho_2,\theta,z_2)=0, \quad (9.1)$$

$$E_y(\rho_2,\theta,z_2)=\frac{(-i)^{2n}k^2z_1z_2}{r_2^2}\exp\left[i(n\theta+kr_2)\right]A_{11}\times$$
$$\times\int_0^{a_1}\frac{G1_{0n}(\rho_1,z_1)}{r_1^2}\exp\left[ik\left(r_1+\frac{\rho_1^2}{2r_2}\right)\right]J_n(x)U(\rho_1)\rho_1 d\rho_1, \quad (9.2)$$

$$E_z(\rho_2,\theta,z_2)=\frac{(-i)^{2n}k^2z_1}{r_2^2}\exp\left[i(n\theta+kr_2)\right]A_{11}\times$$
$$\times\int_0^{a_1}\frac{G1_{0n}(\rho_1,z_1)}{r_1^2}\exp(ikr_1)\times\left\{\begin{array}{l}\rho_2\sin\theta\,J_n(x)+\\+\dfrac{\rho_1}{2}\left[\begin{array}{l}\exp(i\theta)J_{n+1}(x)+\\+\exp(-i\theta)J_{n-1}(x)\end{array}\right]\end{array}\right\}\times$$
$$\times\exp\left(ik\frac{\rho_1^2}{2r_2}\right)U(\rho_1)\rho_1 d\rho_1, \quad (9.3)$$

where (ρ_2,θ,z_2) are the cylindrical coordinates in the focal region of the lens, $r_2=\sqrt{\rho_2^2+z_2^2}$, and $x=\frac{k\rho_1\rho_2}{r_2}$. The field components for the azimuthally polarized TE_{01} mode at a distance z_2 from the lens have the following form:

$$E_x(\rho_2,\theta,z_2)=\frac{(-i)^{2n+3}k^2z_1z_2}{2r_2^2}\exp\left[i(n\theta+kr_2)\right]B_{01}\times$$
$$\times\int_0^{a_1}\left[\begin{array}{l}\exp(i\theta)G2_{1n+1}(\rho_1,z_1)J_{n+1}(x)-\\-\exp(-i\theta)G2_{1n-1}(\rho_1,z_1)J_{n-1}(x)\end{array}\right]\times$$
$$\times\frac{\exp\left[ik\left(r_1+\frac{\rho_1^2}{2r_2}\right)\right]}{r_1^2}U(\rho_1)\rho_1 d\rho_1, \quad (10.1)$$

$$E_y(\rho_2,\theta,z_2)=\frac{(-i)^{2n}k^2z_1z_2}{2r_2^2}\exp\left[i(n\theta+kr_2)\right]B_{01}\times$$
$$\times\int_0^{a_1}\left[\begin{array}{l}\exp(i\theta)G2_{1n+1}(\rho_1,z_1)J_{n+1}(x)+\\+\exp(-i\theta)G2_{1n-1}(\rho_1,z_1)J_{n-1}(x)\end{array}\right]\times$$
$$\times\frac{\exp\left[ik\left(r_1+\frac{\rho_1^2}{2r_2}\right)\right]}{r_1^2}U(\rho_1)\rho_1 d\rho_1, \quad (10.2)$$

$$E_z(\rho_2,\theta,z_2)=\frac{(-i)^{n}k^2z_1}{2r_2^2}\exp\left[i(n\theta+kr_2)\right]B_{01}\times$$
$$\times\int_0^{a_1}\left\{\begin{array}{l}\rho_2\exp(-i\theta)\left[\begin{array}{l}G2_{1n+1}(\rho_1,z_1)\exp(i\theta)(-i)^{n+1}J_{n+1}(x)+\\+G2_{1n-1}(\rho_1,z_1)\exp(-i\theta)(-i)^{n-1}J_{n-1}(x)\end{array}\right]+\\+\rho_1\left[\begin{array}{l}G2_{1n+1}(\rho_1,z_1)(-i)^{n+2}J_n(x)+\\+G2_{1n-1}(\rho_1,z_1)\exp(-2i\theta)(-i)^{n}J_{n-2}(x)\end{array}\right]\end{array}\right\}\times$$
$$\times\frac{\exp\left[ik\left(r_1+\frac{\rho_1^2}{2r_2}\right)\right]}{r_1^2}U(\rho_1)\rho_1 d\rho_1, \quad (10.3)$$

3. Calculation results and discussion

Using the expressions (9) and (10) obtained above, we calculated the longitudinal and transverse distributions of the total field intensity $\left(I=|E_x|^2+|E_y|^2+|E_z|^2\right)$ and phase ($\varphi=\mathrm{arctg}(\mathrm{Im}(E_i)/\mathrm{Re}(E_i))$, i = x, y, z) for laser radiation beams formed by the modes of the dielectric waveguide resonator of a terahertz laser during their interaction with SPP and tight focusing in a free space. The calculations were carried out for the axisymmetric linearly polarized EH_{11} mode and the azimuthally polarized TE_{01} mode. The transverse distributions of the field intensity and phase for the longitudinal component are not provided due to their insignificant influence on the total radiation intensity [43]. The radiation wavelength in the calculations was λ = 432.6 μm (the generation line of an HCOOH THz laser with optical pumping). The waveguide diameter was $2a_1$ = 35 mm. SPP with an aperture of the same diameter was placed at the waveguide output. In this case, the topological charge n of SPP was equal to 0, 1, and 2. The diameter of the lens was $2a_2$ = 50 mm. The focal length of the lens F was selected in accordance with the condition of tight focusing [44] (numerical aperture of the lens NA = 0.69). For complete beam interception, the distance between the SPP and the lens was z_1 = 300 mm. The calculation results are shown in Figs. 2 to 7.

Fig. 2 shows the distributions of the field intensity of the linearly polarized EH_{11} mode along the z axis with tight focusing for the SPP topological charges n = 0, 1, and 2. Calculations of the diameters d and the lengths l_z of the focal region along the z axis for the studied beams were carried out at a maximum field intensity equal to 0.5. Note that the initial EH_{11} mode at n = 0 is focused into a spot with a diameter d = 0.51 mm at a distance z = 37.1 mm from the lens plane. The length of the focal area is l_z = 3.3 mm. The vortex beam at n = 1 is focused into a ring with a diameter d = 1.21 mm at a distance z = 37.4 mm. The length of the focal region is l_z = 4.2 mm. The vortex beam at n = 2 is focused into a ring with a diameter d = 1.57 mm at a distance z = 39.05 mm. The length of the focal area is l_z = 5.8 mm. The hollow channel in the tubular structure of the focal region for n = 0 and n = 2 has local expansions near the focal plane.

It can be seen from Fig. 2 that at the topological charge of SPP n = 0, the mode under study has a maximum radiation intensity on the axis. Introduction of the topological charge n = 1 results in a minimum radiation intensity on the axis as well as an increase in the size of the focal spot. Increasing the topological charge to n = 2 further increases the size of the focal spot.

The field intensity and phase distributions in the cross-section of the focal region of the lens for the field component E_y in the case of the topological charges n = 0, 1, and 2 are shown in Fig. 3. These distributions are plotted in the region of the maximum field intensity.

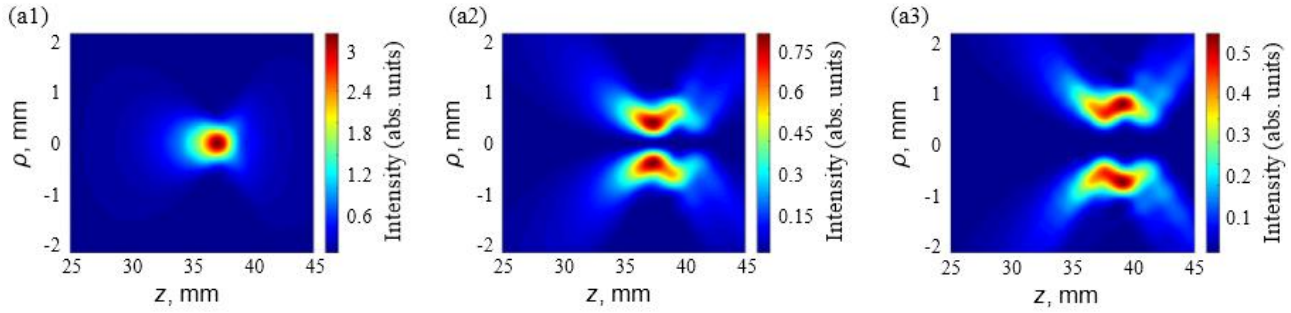

Fig. 2. Calculated longitudinal distributions of the field intensity of the EH_{11} mode in the lens focal region for the topological charges $n = 0$ (a1), 1 (a2), and 2 (a3). (Color online)

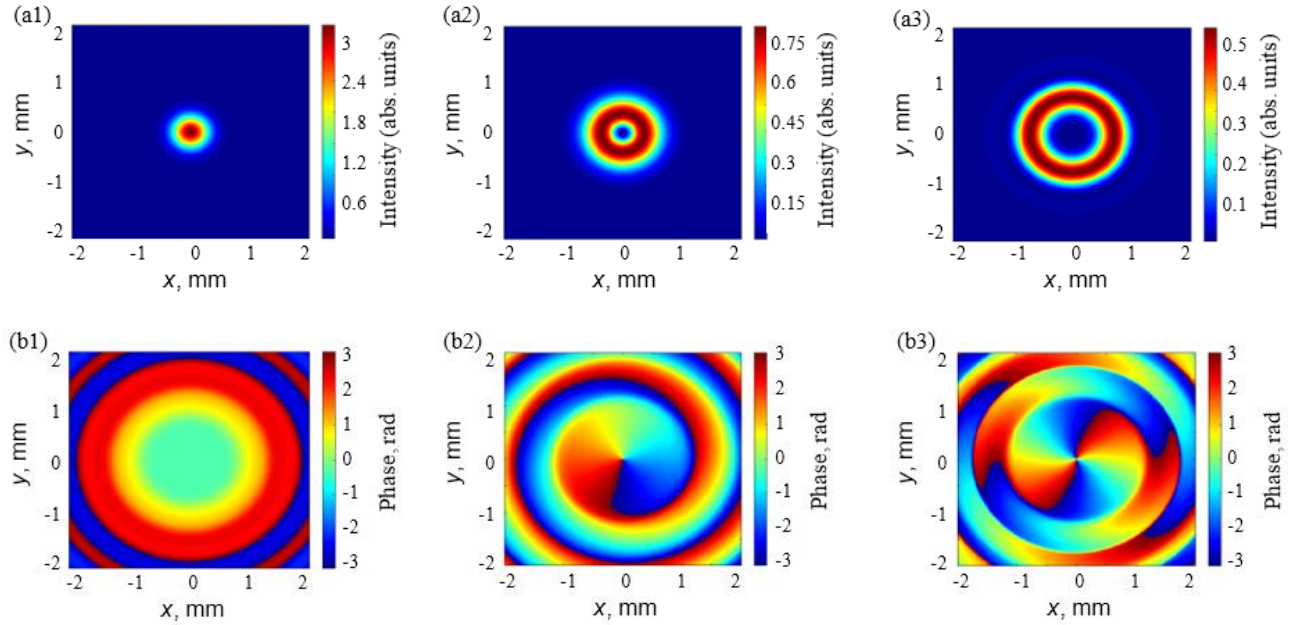

Fig. 3. Calculated transverse distributions of the field intensity (a1 – a3) and phase (b1 – b3) of the field component E_y for the EH_{11} mode in the lens focal region for the topological charges $n = 0$ (a1, b1), 1 (a2, b2), and 2 (a3, b3). (Color online)

It can be seen from this figure that the wavefront in the focal region of the lens transforms from spherical to spiral with increasing the topological charge. A vortex beam with the charge $n = 1$ has one helical branch and a vortex beam with the charge $n = 2$ has two helical branches. The phase singularity points are located in the minimum of the field intensity.

Fig. 4 shows the field intensity distributions along the z axis of the azimuthally polarized TE_{01} mode with tight focusing for the topological charges $n = 0$, 1, and 2. Note that the original TE_{01} mode ($n = 0$) is focused into a ring with a diameter $d = 1.08$ mm and the length of the focal region is $l_z = 3.35$ mm. The vortex beam with $n = 1$ is focused into a spot with a diameter $d = 0.45$ mm. Here, the extension of the focal region is $l_z = 3.05$ mm. The vortex beam at $n = 2$ is focused into a ring with a diameter $d = 1.32$ mm. The length of the focal region is $l_z = 4.75$ mm. The hollow channel in the tubular structure of the focal region for $n = 0$ and $n = 2$ has no local expansions near the focal plane. For all the topological charges, the area of the maximum intensity is formed at the same distance from the lens, $z = 37.25$ mm. It can be seen from Fig. 4 that at the topological charges $n = 0$ and $n = 2$ the intensity distribution retains a ring shape, and at $n = 1$ the beam profile becomes Gaussian-like.

Fig. 5 shows the calculated transverse distributions of the field intensity and phase for individual radiation components of the TE_{01} mode in the focal region of the lens for the topological charges $n = 0$, 1, and 2. It can be seen from this figure that a vortex beam with the charge $n = 1$ has two helical branches and a vortex beam with the charge $n = 2$ has three helical branches. The points of phase singularity are located in the field intensity minimum.

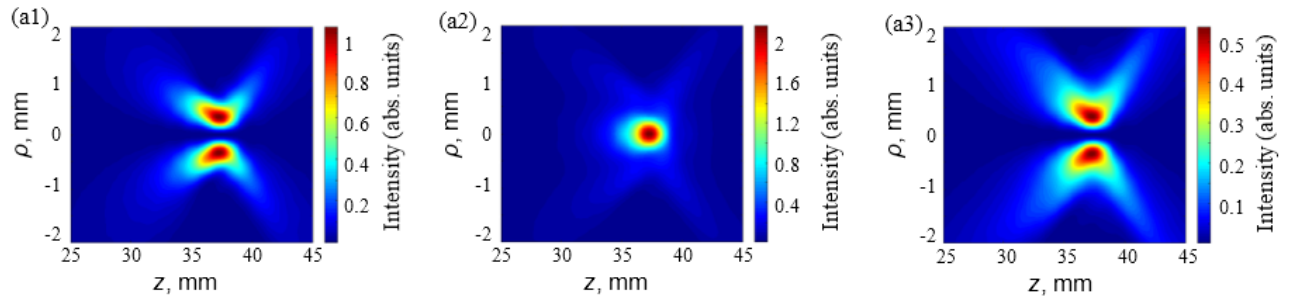

Fig. 4. Calculated longitudinal distributions of the field intensity of the TE_{01} mode in the lens focal region for the topological charges n = 0 (a1), 1 (a2), and 2 (a3). (Color online)

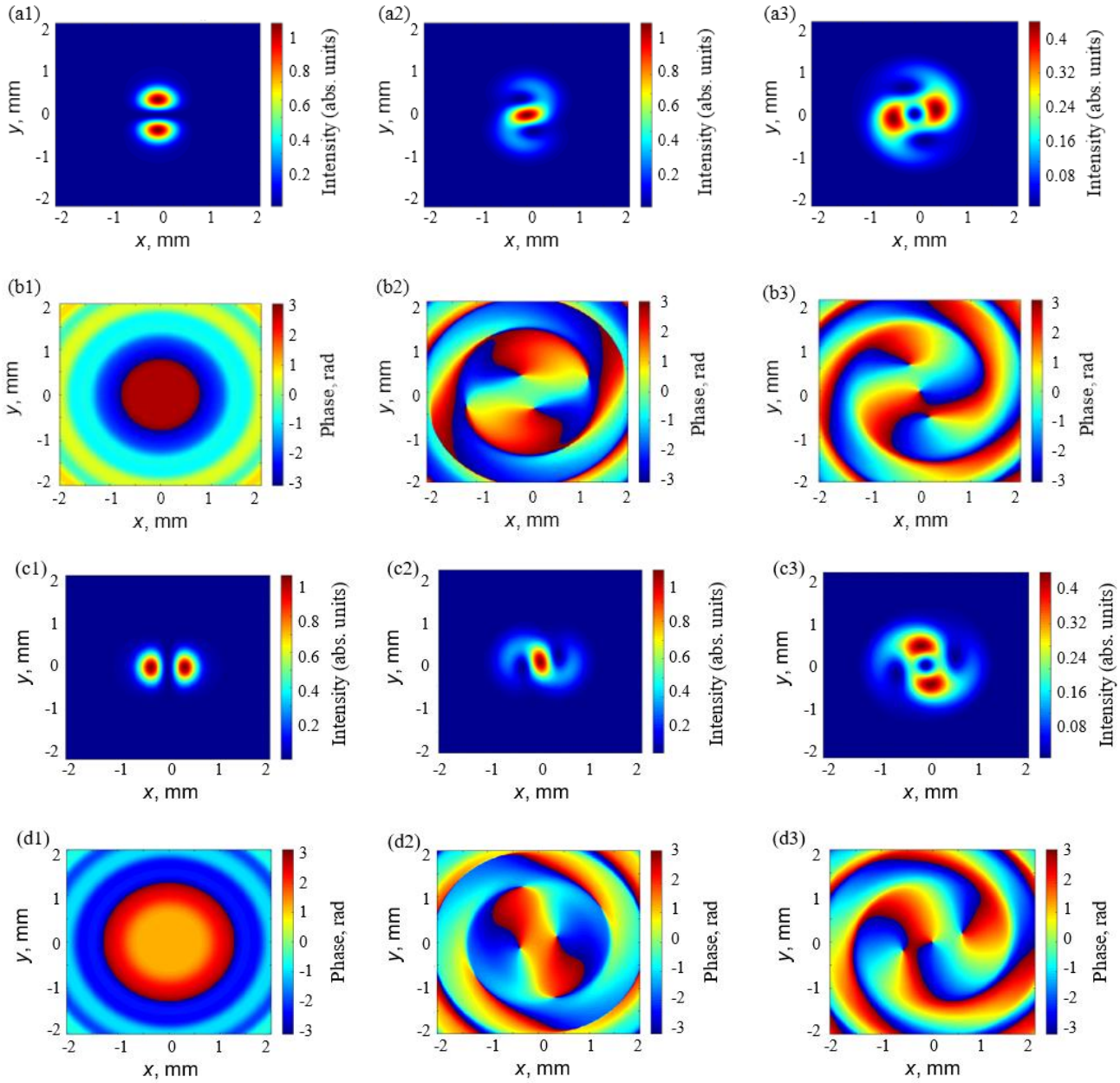

Fig. 5. Calculated transverse intensity (a1 – a3, c1 – c3) and phase (b1 – b3, d1 – d3) distributions for the field components E_x (a1 – a3, b1 – b3) and E_y (c1 – c3, d1 – d3) of the TE_{01} mode in the focal region of the lens for the topological charges n = 0 (first column), 1 (second column) and 2 (third column). (Color online)

4. Conclusions

In this paper, the wave characteristics of vortex laser beams at their tight focusing are investigated using the Rayleigh–Sommerfeld vector theory. The laser beams were formed by the modes of a waveguide dielectric resonator of a terahertz laser.

It is shown that at the topological charge of SPP $n = 0$, the studied EH_{11} mode has a maximum of the radiation intensity on the axis. Introduction of a topological charge leads to appearance of a minimum of radiation intensity on the axis as well as to increase in the size of the focal spot. However, for the TE_{01} mode with the topological charges $n = 0$ and $n = 2$, the intensity distribution retains a ring shape, and at $n = 1$ the beam profile turns into the Gaussian-like one. It should be noted that for all the topological charges, the region of the field intensity maximum for the TE_{01} mode is formed at the same distance from the lens, in contrast to the EH_{11} mode.

The wave front in the focal region of the lens for the components of the EH_{11} and TE_{01} modes transforms from spherical to spiral one with increasing the topological charge. The vortex beam for the component E_y of EH_{11} mode with the charge $n = 1$ has one helical branch and with the charge $n = 2$ two helical branches. For the transverse components of the TE_{01} mode, two and three helical branches are observed, respectively. The points of phase singularity both for the components of the EH_{11} and TE_{01} modes are located in the minimum of the field intensity.

References

1. Headland D., Monnai Y., Abbott D. *et al*. Tutorial: Terahertz beam forming, from concepts to realizations. *APL Photonics*. 2018. **3**. P. 051101. https://doi.org/10.1063/1.5011063.
2. Youngworth K.S., Brown T.G. Focusing of high numerical aperture cylindrical-vector beams. *Opt. Exp*. 2000. **7**. P. 77–87. https://doi.org/10.1364/OE.7.000077.
3. Choporova Y., Knyazev B., Mitkov M. *et al*. Simulation of propagation and transformation of THz Bessel beams with orbital angular momentum. *Phys. Procedia*. 2016. **84**. P. 175–183. https://doi.org/10.1016/j.phpro.2016.11.031.
4. Forbes A. Advances in orbital angular momentum lasers. *J. Lightwave Technol*. 2023. **41**. P. 2079–2086. https://doi.org/10.1109/JLT.2022.3220509.
5. Wang H., Song Q., Cai Y. *et al.* Recent advances in generation of terahertz vortex beams and their applications. *Chin. Phys. B*. 2020. **29**. P. 097404. https://doi.org/10.1088/1674-1056/aba2df.
6. Petrov N.V., Sokolenko B., Kulya M.S. *et al.* Design of broadband terahertz vector and vortex beams: I. Review of materials and components. *Light: Advanced Manufacturing*. 2022. **3**. P. 640–652. https://doi.org/10.37188/lam.2022.043.
7. Nagatsuma T., Ducournau G., Renaud C.C. Advances in terahertz communications accelerated by photonics. *Nat. Photonics*. 2016. **10**. P. 371–379. https://doi.org/10.1038/nphoton.2016.65.
8. Chen S.C., Feng Z., Li, J. *et al.* Ghost spintronic THz-emitter-array microscope. *Light Sci. Appl*. 2020. **9**. P. 99. https://doi.org/10.1038/s41377-020-0338-4.
9. Nobahar D., Khorram S. Terahertz vortex beam propagation through a magnetized plasma-ferrite structure. *Opt. Laser Technol*. 2022. **146**. P. 107522. https://doi.org/10.1016/j.optlastec.2021.107522.
10. Hibberd M.T., Healy A.L., Lake D.S. *et al.* Acceleration of relativistic beams using laser generated terahertz pulses. *Nat. Photonics*. 2019. **14**. P. 755–759. https://doi.org/10.1038/s41566-020-0674-1.
11. Klug A., Nape I., Forbes A. The orbital angular momentum of a turbulent atmosphere and its impact on propagating structured light fields. *New J. Phys*. 2021. **23**. P. 093012. https://doi.org/10.1088/1367-2630/ac1fca.
12. Pinnock S.W., Roh S., Biesner T. *et al.* Generation of THz vortex beams and interferometric determination of their topological charge. *IEEE Trans. Terahertz Sci. Technol*. 2022. **13**. P. 44–49. https://doi.org/10.1109/TTHZ.2022.3221369.
13. Rubano A., Cardano F., Piccirillo B., Marrucci L. Q-plate technology: a progress review [Invited]. *J. Opt. Soc. Am. B*. 2019. **36**. P. D70–D87. https://doi.org/10.1364/JOSAB.36.000D70.
14. Imai R., Kanda N., Higuchi T. *et al*. Generation of broadband terahertz vortex beams. *Opt. Lett*. 2014. **39**. P. 3714–3717. https://doi.org/10.1364/OL.39.003714.
15. Yang Y., Ye X., Niu L. *et al.* Generating terahertz perfect optical vortex beams by diffractive elements. *Opt. Express*. 2020. **28**. P. 1417–1425. https://doi.org/10.1364/OE.380076.
16. Zhang K., Wang Y., Burokur S.N., Wu Q. Generating dual-polarized vortex beam by detour phase: from phase gradient metasurfaces to metagratings. *IEEE Trans. Microw. Theory Techn.* 2022. **70**. P. 200–209. https://doi.org/10.1109/TMTT.2021.3075251.
17. Zhang X.D., Su Y.H., Ni J.C. *et al.* Optical superimposed vortex beams generated by integrated holographic plates with blazed grating. *Appl. Phys. Lett*. 2017. **111**. P. 061901. https://doi.org/10.1063/1.4997590.
18. Ge S.J., Shen Z.X., Chen P. *et al.* Generating, separating and polarizing terahertz vortex beams via liquid crystals with gradient-rotation directors. *Crystals*. 2017. **7**. P. 314. https://doi.org/10.3390/cryst7100314.
19. Guan S., Cheng J., Chang S. Recent progress of terahertz spatial light modulators: materials, principles and applications. *Micromachines*. 2022. **13**. P. 1637. https://doi.org/10.3390/mi13101637.
20. Al Dhaybi A., Degert J., Brassele E. *et al*. Terahertz vortex beam generation by infrared vector beam rectification. *JOSA B*. 2019. 3**6**. P. 12–18. https://doi.org/10.1364/JOSAB.36.000012.

21. Miyamoto K., Sano K., Miyakawa T. *et al.* Generation of high-quality terahertz OAM mode based on soft-aperture difference frequency generation. *Opt. Express*. 2019. **27**. P. 31840–31849. https://doi.org/10.1364/OE.27.031840.
22. Sobhani H., Dadar E. Terahertz vortex generation methods in rippled and vortex plasmas. *JOSA A*. 2019. **36**. P. 1187–1196. https://doi.org/10.1364/JOSAA.36.001187.
23. Beijersbergen M.W., Coerwinkel R.P.C., Kristensen M., Woerdman J.P. Helical-wavefront laser beams produced with a spiral phase plate. *Opt. Commun*. 1994. **112**. P. 321–327. https://doi.org/10.1016/0030-4018(94)90638-6.
24. Nicolas A., Veissier L., Giner L. *et al.* A quantum memory for orbital angular momentum photonic qubits. *Nat. Photonics*. 2014. **8.** P. 234–238. https://doi.org/10.1038/nphoton.2013.355.
25. Tamburini F., Thidé B., Molina-Terriza G. *et al.* Twisting of light around rotating black holes. *Nat. Phys.* 2011. **7**. P. 195–197. https://doi.org/10.1038/nphys1907.
26. Meier M., Romano V., Feurer T. Material processing with pulsed radially and azimuthally polarized laser radiation. *Appl. Phys. A*. 2007. **86**. P. 329–334. https://doi.org/10.1007/s00339-006-3784-9.
27. Simpson N.B., Dholakia K., Allen L., Padgett M.J. Mechanical equivalence of spin and orbital angular momentum of light: an optical spanner. *Opt. Lett.* 1997. **22**. P. 52–54. https://doi.org/10.1364/OL.22.000052.
28. Rao L., Pu J., Chen Z., Yei P. Focus shaping of cylindrically polarized vortex beams by a high numerical-aperture lens. *Opt. Laser Technol*. 2009. **41**. P. 241–246. https://doi.org/10.1016/j.optlastec.2008.06.012.
29. Pu J., Zhang Z. Tight focusing of spirally polarized vortex beams. *Opt. Laser Technol*. 2010. **42**. P. 186–191. https://doi.org/10.1016/j.optlastec.2009.06.008.
30. Youngworth K.S., Brown T.G. Focusing of high numerical aperture cylindrical-vector beams. *Opt. Express*. 2000. **7**. P. 77–87. https://doi.org/10.1364/oe.7.000077.
31. Han L., Liu S., Li P. *et al.* Catalyst-like effect of orbital angular momentum on the conversion of transverse to three-dimensional spin states within tightly focused radially polarized beams. *Phys. Rev. A*. 2018. **97**. P. 053802. https://doi.org/10.1103/PhysRevA.97.053802.
32. Li H., Ma C., Wang J. *et al.* Spin-orbit Hall effect in the tight focusing of a radially polarized vortex beam. *Opt. Express*. 2021. **29**. P. 39419–39427. https://doi.org/10.1364/OE.443271.
33. Zhang X., Shen B., Zhu Z. *et al.* Understanding of transverse spin angular momentum in tightly focused linearly polarized vortex beams. *Opt. Express.* 2022. **30**. P. 5121–5130. https://doi.org/10.1364/OE.449583.
34. Li M., Cai Y., Yan S. *et al.* Orbit-induced localized spin angular momentum in strong focusing of optical vectorial vortex beams. *Phys. Rev. A.* 2018. **97**. P. 053842. https://doi.org/10.1103/PhysRevA.97.053842.
35. Zhang X., Xu Y., Hong B. *et al.* Generation of a focused THz vortex beam from a spintronic THz emitter with a helical Fresnel zone plate. *Nanomaterials*. 2023. **13**. P.2037. https://doi.org/10.3390/nano13142037.
36. Li H., Zheng C., Xu H. *et al.* All-graphene geometric terahertz metasurfaces for generating multi-dimensional focused vortex beams. *Opt. Laser Technol*. 2023. **159**. P. 108986. https://doi.org/10.1016/j.optlastec.2022.108986.
37. Chevalier P., Amirzhan A., Wang F. *et al.* Widely tunable compact terahertz gas lasers. *Science*. 2019. **366**. P. 856–860. https://doi.org/10.1126/science.aay8683.
38. Farhoomand J., Pickett H.M. Stable 1.25 watts CW far infrared laser radiation at the 119 μm methanol line. *Int. J. Infrared Milli. Waves*. 1987. **8**. P. 441–447. https://doi.org/10.1007/BF01013257.
39. Marcatili E.A.J., Schmeltzer R.A. Hollow metallic and dielectric waveguides for long distance optical transmission and lasers. *Bell Syst. Tech. J.* 1964. **43**. P. 1783–1809. https://doi.org/10.1002/j.1538-7305.1964.tb04108.x.
40. Zhang Y., Wang L., Zheng C. Vector propagation of radially polarized Gaussian beams diffracted by an axicon. *J. Opt. Soc. Am. A*. 2005. **22**. P. 2542–2546. https://doi.org/10.1364/JOSAA.22.002542.
41. Nye J.F., Berry M.V. Dislocations in wave trains. *Proc. R. Soc. Lond. A. Math. Phys. Sci*. 1974. **336**. P. 165–190. https://doi.org/10.1098/rspa.1974.0012.
42. Gu B., Cui, Y. Nonparaxial and paraxial focusing of azimuthal-variant vector beams. *Opt. Express*, 2012. **20**. P. 17684–17694. https://doi.org/10.1364/OE.20.017684.
43. Gurin O.V., Degtyarev A.V., Dubinin M.M. *et al.* Focusing of modes with an inhomogeneous spatial polarization of the dielectric resonator of a terahertz laser. *Telecommunications and Radio Engineering*. 2020. **79**. P. 105–116. https://doi.org/10.1615/TelecomRadEng.v79.i2.30.
44. Chen Z., Hua L., Pu J. Tight focusing of light beams: Effect of polarization, phase and coherence. *Prog. Opt.* 2012. **57**. P. 219–260. https://doi.org/10.1016/B978-0-44-459422-8.00004-7.

Authors' contributions

Degtyarev A.V.: formal analysis, project administration, writing – review & editing.

Dubinin M.M.: methodology, investigation, writing – review & editing.

Maslov V.A.: formal analysis, conceptualization, investigation, writing – original draft, writing – review & editing.

Muntean K.I.: validation, formal analysis

Svystunov O.O.: investigation, formal analysis.

Authors and CV

Andrey V. Degtyarev, PhD in Physics and Mathematics, Associate Professor, Department of Quantum Radiophysics, School of Radiophysics, Biomedical Electronics and Computer System, V.N. Karazin Kharkiv National University. Authored more than 80 scientific works, several methodical training manuals, three monographs, and a patent for an invention. The field of his scientific interests is laser physics, laser optics, and propagation of laser radiation beams in electromagnetic energy transmission lines.
E-mail: a.v.degtyarev@karazin.ua,
https://orcid.org/0000-0003-0844-4282

Mykola M. Dubinin, PhD in Applied Physics and Nanomaterials, Department of Quantum Radiophysics, School of Radiophysics, Biomedical Electronics and Computer System, V.N. Karazin Kharkiv National University. He is the author of more than 30 scientific works. The field of his scientific interests is laser physics, laser optics, and propagation, focusing and control of laser radiation beams.
https://orcid.org/0000-0002-7723-9592

Vyacheslav O. Maslov, Doctor of Physical and Mathematical Sciences, Professor, Head of the Department of Quantum Radiophysics, School of Radiophysics, Biomedical Electronics and Computer System, V.N. Karazin Kharkiv National University. He is the author of more than 180 scientific works, 6 monographs, several methodical training manuals, and 16 copyright certificates for inventions and patents. The field of his scientific interests is laser physics, laser optics, and propagation of laser radiation beams in electromagnetic energy transmission lines.
E-mail: v.a.maslov@karazin.ua,
https://orcid.org/0000-0001-7743-7006

Konstantin I. Muntean, Researcher, Department of Quantum Radiophysics, School of Radiophysics, Biomedical Electronics and Computer System, V.N. Karazin Kharkiv National University. He is the author and co-author of more than 90 scientific publications, including 14 copyright certificates and patents for inventions. The field of his scientific interests is measurements and stabilization of laser radiation parameters. E-mail: k.i.muntean@karazin.ua,
https://orcid.org/0000-0001-6479-3511

Oleh O. Svystunov, PhD Student, Department of Quantum Radiophysics, School of Radiophysics, Biomedical Electronics and Computer System, V.N. Karazin Kharkiv National University. He is the author of 7 scientific works. The field of his scientific interests is laser physics, laser optics, propagation and focusing of laser radiation beams.
E-mail: oleg.svistunov.98@gmail.com,
https://orcid.org/0000-0002-4967-5944

Гостре фокусування терагерцових вихрових пучків, сформованих лазерним діелектричним резонатором

А.В. Дегтярьов, М.М. Дубінін, В.О. Маслов, К.І. Мунтян, О.О. Свистунов

Анотація. Теоретично досліджено хвильові характеристики вихрових лазерних пучків при їх гострому (жорсткому) фокусуванні. Для опису поширення у вільному просторі лазерних пучків, збуджених модами хвилевідного діелектричного резонатора, було використано теорію Релея–Зоммерфельда. Показано, що при топологічному заряді спіральної фазової пластини $n = 0$ досліджувана мода EH_{11} має максимум інтенсивності випромінювання на осі. Введення топологічного заряду n приводить до виникнення мінімуму інтенсивності випромінювання на осі, а також до збільшення розміру фокальної плями. Однак для моди TE_{01} при топологічних зарядах $n = 0$ та $n = 2$ розподіл інтенсивності зберігає кільцеподібну форму, а при $n = 1$ профіль пучка переходить у гауссівський. Хвильовий фронт у фокальній області лінзи для компонент мод EH_{11} та TE_{01} перетворюється зі сферичного на спіральний зі збільшенням топологічного заряду.

Ключові слова: вихрові пучки, терагерцовий лазер, діелектричний резонатор, моди, гостре фокусування.